Materials and Design 30 (2009) 1913–1921

Contents lists available at ScienceDirect

Materials and Design

journal homepage: www.elsevier.com/locate/matdes

Influence of friction stir welding parameters on the microstructural and mechanical properties of AA 6016-T4 thin welds

D.M. Rodrigues [a,*], A. Loureiro [a], C. Leitao [a], R.M. Leal [a,b], B.M. Chaparro [a,c], P. Vilaça [d]

[a] CEMUC, Department of Mechanical Engineering, University of Coimbra, 3030-788 Coimbra, Portugal
[b] ESAD.CR, Polytechnic Institute of Leiria, Caldas da Rainha, Portugal
[c] ESTA, Polytechnic Institute of Tomar, Abrantes, Portugal
[d] IST, Technical University of Lisbon, Lisbon, Portugal

ARTICLE INFO

Article history:
Received 21 July 2008
Accepted 9 September 2008
Available online 21 September 2008

Keywords:
Taylor welded blanks
Friction stir welding
Aluminium alloys, Thin sheets

ABSTRACT

In present work friction stir welds produced in 1 mm thick plates of AA 6016-T4 aluminium alloy, with two different tools, were analysed and compared concerning the microstructure and mechanical properties. For each tool, the welding parameters were optimized in order to achieve non-defective welds. Assuming a relation between the welding parameters and the energy input per unit of length of the weld [Seidel TU, Reynolds AP. Visualization of the material flow in AA2195 friction stir welds using a marker insert technique. Metall Mater Trans A 2001;32A:2879–84; Sato YS, Urata M, Kokawa H. Parameters controlling microstructure and hardness during friction stir welding of precipitation-hardenable aluminum alloy 6063. Metall Mater Trans A 2002;33(3):625–35; Lim S, Kim S, Lee CG, Kim S-J. Tensile behavior of friction-stri-welded Al 6061-T651. Metall Mater Trans A 2004;35(9):2829–35; Yang B, Yan J, Sutton MA, Reynolds AP. Banded microstructure in AA2024-T351 and AA2524-T351 aluminum friction stir welds: Part I. Metallurgical studies. Mater Sci Eng A 2004;364(1–2):55–65; Peel MJ, Steuwer A, Withers PJ, Dickerson T, Shi Q, Shercliff H. Dissimilar friction stir welds in AA5083–AA6082. Part I: process parameter effects on thermal history and weld properties. Metall Mater Trans A 2006;37:2183–193; Gerlich A, Su P, Yamamoto M, North TH. Effect of welding parameters on the strain rate and microstructure of friction stir spot welded 2024 aluminum alloy. J Mater Sci 2007;42(14):5589–601; Lombard H, Hattingh DG, Steuwer A, James MN. Optimising FSW process parameters to minimise defects and maximise fatigue life in 5083-H321 aluminum alloy. Eng Fract Mech 2008;75(3–4):341–54], the welds produced were classified as "hot" and "cold welds". The results obtained showed that the "hot" welds, obtained with the maximum tool rotational speed and the minimum traverse speed, have improved mechanical properties relative to the "cold" welds that were in undermatch condition relative to the base material. The differences in mechanical properties between the two types of welds are explained based in TEM microstructural analysis. Despite the undermatched characteristics of the "cold" welds relative to the base material, formability tests demonstrated that these welds improve the drawing performance of the welded sheets.

1. Introduction

In our days, friction stir welding (FSW) appears as a promisingly ecologic weld method that enables to diminish material waste and to avoid radiation and harmful gas emissions usually associated with the fusion welding processes. This welding technique makes use of a nonconsumable welding tool to generate heat, by friction between it and the faying plates, and to induce strong plastic deformation of the workpiece material promoting its complex mixing across the joint. Detailed description of the process can be found in the literature [8,9].

Although currently FSW can be used to join several materials such as magnesium [10,11], copper [12–14], steel [15–18], titanium [19,20] and MMCs [21,22], the primary research and industrial interest for this process was for butt and lap joining of aluminium alloys, especially the 2XXX, 6XXX and 7XXX series of heat treatable aluminium alloys, usually considered to be "unweldable". Concerning the FSW of the 6XXX series of aluminium alloys, the 6061 series was the most studied, either in similar [3,23–31] and dissimilar [32–40] welding combinations. Large effort was also spent in studding the FSW of the 6082 [5,28,41–47], 6063 [2,48–51], 6056 [52–54], 6022 [55,56], 6005 [57,58], 6013 [59] and 6016 [60] series of alloys. In most of these studies the thicknesses of the plates joined ranged from 3 to 6 mm and only few of them focused in the FSW of very thin plates, less than 2 mm thick [40,44,45,60].

* Corresponding author. Tel.: +351 239 790 700; fax: +351 239 790 701.
E-mail address: dulce.rodrigues@dem.uc.pt (D.M. Rodrigues).

0261-3069/$ - see front matter © 2008 Elsevier Ltd. All rights reserved.
doi:10.1016/j.matdes.2008.09.016

It is also important to enhance that most of the previous works were developed using the alloys in artificially aged temper conditions (mainly T5 and T6 temper conditions) and only a few of them focuses on friction stir welding of the naturally aged alloys (T4). From the analysis of FSW in these materials it was concluded that the mechanical properties of the FS welds depend mainly on the size, volume fraction and distribution of precipitates in the TMAZ and HAZ. In the as-welded condition, softening was detected in the welds for all the artificially aged alloys [2,3,23,26–31,44,45, 49,52,53,56–58]. For the naturally aged alloys, the hardness in the welds remained similar to the base material values [2,59]. In fact, meanwhile the stir zone of the T4 temper alloys maintain the precipitation features of the base material, for the artificially aged alloys, dissolution of thin precipitates occurs during welding [54,59]. For these alloys, frequently, softening is more pronounced in the HAZ than in the TMAZ [3,16,43,44,49,57]. The higher hardness values in the TMAZ relative to the HAZ was attributed to the occurrence of natural aging in the TMAZ after welding, since the temperature reached in this zone during the welding process can be as high as the solutionizing temperature of the precipitates [35,43].

Some authors analysed the influence of the tool rotation speed [2], welding speed [57,58] and both parameters simultaneously [3,5,31,43] on the microstructure and mechanical properties of 6XXX welds. These works enhance the difficulty in evaluating the dependence of the thermal input and mechanical properties on weld parameters. Despite some of the results indicate that increasing rotating speed of the tool or decreasing the welding speed, decreases the lowest hardness value in the hardness profile for the artificially aged alloys [3,43,57,58], some others did not report any hardness change with varying tool rotation rate [2,44]. The influence of tool shoulder [44] and pin [24] geometries in the weld characteristics was also analysed. It was concluded that the shoulder geometry is more determinant in conditioning the weld properties than pin geometry.

The base metal (BM) used in this study was the AA 6016 aluminium alloy supplied in 1.0 mm thick rolled plates, heat-treated and naturally aged to a T4 stable condition. This alloy, in the T4 condition, has good hemming properties, good weldability, very good corrosion resistance and very good formability with no stretcher strain marks, which makes it ideal for car skin sheet applications. In present work FS welds, produced with two different tools, are analysed and compared concerning microstructure and mechanical properties. For each tool, the welding parameters were previously optimized in order to achieve non-defective welds. The results presented in this paper indicate that the optimized welds have very different characteristics concerning material mixing and mechanical behaviour. Comparing present results with that obtained for other 6XXX alloys, the importance of the initial temper condition of the alloy and the welding parameters, in the weld characteristics, is enhanced.

2. Welding procedure

In the present work, welds in 1 mm thick sheets of the automotive AA 6016-T4 aluminium alloy were performed with two different tool shoulder geometries: a conical shoulder with a 8° inclination cavity and 10 mm in diameter (Tool 1, Fig. 1a) and a scrolled shoulder with 14 mm in diameter (Tool 2, Fig. 1b). The geometry of the probe was the same for both tools, a cylindrical threaded probe with 3 mm in diameter, 1 mm long for the conical shoulder and 0.85 mm long for the scrolled shoulder. The conical shoulder geometry is very traditional and has already been used in numerous applications. The shoulder cavity, in combination with tool tilt angle, enables to compress annular rings of plasticized material around the tool, compelling material flow toward the pin and preventing its removal from the weld. The scrolled shoulder used in this work has two helical flutes that force material flow around the pin, enabling to work without toll tilt angle and to reducing flash formation.

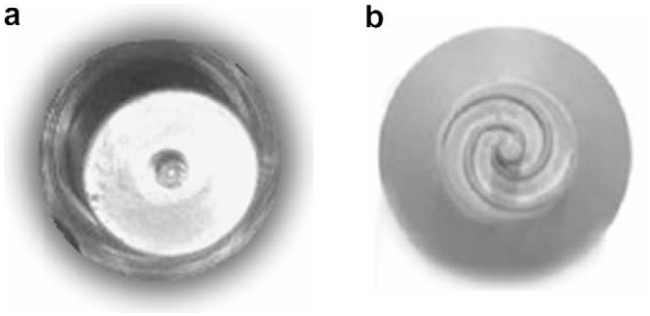

Fig. 1. (a) Tool 1 and (b) Tool 2.

Table 1
Welding parameters

	Welding speed (v)	Rotation speed (ω)	Tool tilt angle
Tool 1 Conical shoulder	180 mm/min	1800 rpm	2.5°
Tool 2 Scrolled Shoulder	320 mm/min	1120 rpm	0°

Friction stir welds were performed parallel to the rolling direction of the plates using a conventional milling machine. The welding parameters used with each tool, that are presented in Table 1, resulted from an optimization work that conducted to defect free welds with good appearance. Since the maximum temperature in the welds was directly related with the rotational and traverse speed of the tool, being currently accepted that the maximum temperature in the welds raise with increasing tool rotation speeds and decreasing traverse speed [2,3], in a first analysis, the welds produced with Tool 1 can be considered as "hot" welds and the welds produced with Tool 2 as "cold" welds. In the text, the "hot" welds will be labelled as HW and the "cold" welds as CW.

3. Testing procedure

The first step in characterizing the welds was a visual inspection and qualitative analysis of the weld roots and crowns. X-ray inspections and bending tests of welded specimens were also carried out to check that no defects like root flaws or kissing bond were present in the welds. Cross-sectioning of the welds for metallographic analysis in planes perpendicular to the welding direction and parallel to the weld crown was also performed. The samples were prepared according to standard metallographic practice and etched with Hatch (macrographs) and Poultons modified (micrographs) reagents in order to enable the identification of the different weld zones. TEM observations were also carried out at various locations in the weld. Thin-foil specimens, with 3-mm diameter, which were cut out from various locations in the weld, were prepared by jet electropolishing in nitric acid/methanol solution. The TEM observations were carried out in a FEI, Tecnai G2, S-Twin microscope.

The heterogeneity in mechanical properties across the welds was evaluated by performing hardness measurements transversely to the weld direction, 0.75 mm from the root face, using a Shimadzu® – Micro-Hardness Tester with 100 gf load for 30 s. In each testing line the hardness measurements were spaced by

intervals of 0.25 mm. The hardness measurements were performed after several weeks of natural aging at room temperature of the welds. All the microhardness results were verified by performing, for each type of sample, hardness measurements in several positions along the welding directions.

In order to evaluate the overall mechanical behaviour of the joints, transverse tensile tests were carried out on an INSTROM Mod. 4206 machine, at room temperature and with a crosshead speed of 5 mm/min. The tensile specimens were machined from the TWBs so that the weld was centred in the gauge section and the tensile axis was normal to the welding direction. None of the tensile samples were flat machined in order to smooth the surface or to make the cross-section area constant along the gage length. Since the main field of application of the AA 6016-T4 alloy is in obtaining sheet metal formed parts, the formability of the welded sheets was analysed by deep-drawing Cylindrical Cups with a stamping tool developed to perform these tests in conventional tensile test equipments [61,62]. Testing conditions were 100 mm/min punch speed and 8 kN clamping force.

4. Results and discussion

4.1. Base material

The nominal composition of the alloy, as indicated by the supplier, is 1–1.5% Si, <0.5% Fe, <0.2% Cu, <0.2% Mn, 0.25–0.6% Mg, <0.2% Zn, <0.15% Ti, <0.1% Cr. A micrograph and a TEM bright field image of the base material are shown in Fig. 2. As it can be seen in this figure, the base material is characterized by a recrystalized microstructure with equiaxed grains, with relatively uniform grain size of 23 μm, as determined by using the mean linear intercept method. In the TEM bright field image of Fig. 2b only coarse precipitates randomly distributed in the grain structure are visible, which is characteristic of long time naturally aged aluminium alloys. In fact, Murayama et al. [17,63] reported that clusters of Mg atoms are present in the Al–Mg–Si as-quenched alloys, and separate clusters of Mg and Si atoms and their co-clusters evolve after long-term natural aging. The presence of β'' or β' phases characteristic of artificially aged alloys, is not expected to occur in the naturally aged alloys [53,54,59,63].

4.2. Microstructural analysis of the welds

Regardless of the welding conditions, the welds analysed in this work were successfully joined and showed no porosity and/or defects in both weld top and root surfaces. The aspect of the weld roots and crowns is shown in Fig. 3a and c, for welds produced with Tool 1 (HW), and in Fig. 3b and d, for welds produced with Tool 2 (CW). As it can be seen in the figure, no flash was produced during welding for both tolls. However, meanwhile the crown of the HW welds is smooth with regularly spaced semi-circular bands, usually associated with tool advance per revolution, for the CW welds, the surface is deeply rough. Due to Tool 1 tilt angle, a 0.1 mm thickness undermatch was measured in the stirred zone of the HW welds relative to base material initial thickness. The thickness reduction across the stirred material is negligible for the CW welds.

In Fig. 4 is shown the macrostructure in the cross-section of HW (Fig. 4a) and CW (Fig. 4b) welds. Although a different grain size structure is discernible in the weld region, the typical FSW onion ring features are not visible, especially for the weld performed with Tool 2. A common feature in both images is the presence of the zigzag oxide layer at the weld nugget, which is a memory of the joint line and can be considered as indicative of low heat input during the welding process [35,40,62]. Comparing both macrographs it is possible to observe that the zigzag layer is much more pronounced and continuous for the cold weld.

In order to enable a better understanding of the microstructure in the nugget region of both welds, which is not easily discernible in this type of similar welds due to the difficulty in achieving a satisfactory etching contrast, the optical microstructures of two dissimilar welds obtained by FSW of 1 mm thick plates of the AA 6016-T4 alloy with AA 5182-H111 alloy, by using the same type of tools and welding parameters of Table 1, are shown in Fig. 5. In Fig. 5a is shown the dissimilar AA 6016–AA 5182 weld, produced with Tool 1 (HD weld), and in Fig. 5b is shown the dissimilar AA 6016–AA 5182 weld, produced with Tool 2 (CD weld). When comparing the HW (Fig. 4a) and HD (Fig. 5a) weld images, the only common features are the sharply defined boundary transition between TMAZ and the HAZ, on the advancing side of the weld, and a gradual transition between these two regions at the retreating side of the welds. Comparing the CW (Fig. 4b) and CD (Fig. 5b)

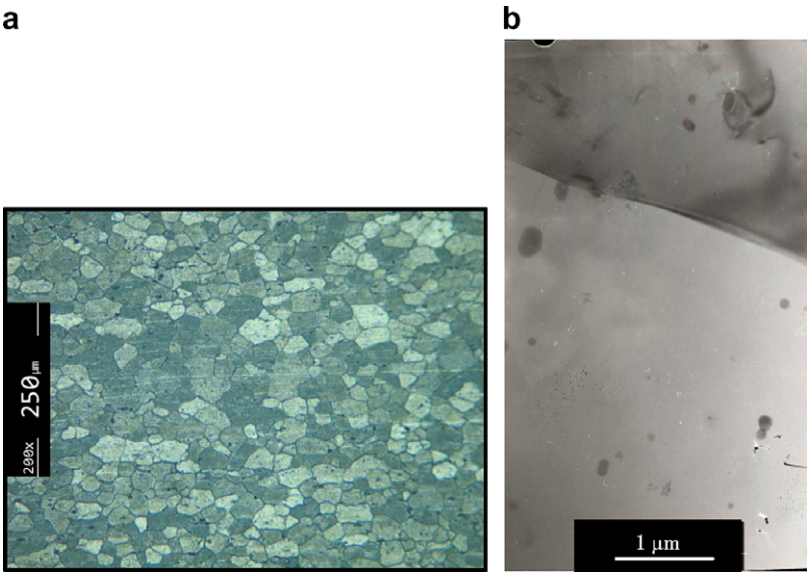

Fig. 2. Optical and TEM microstructures of the AA 6016-T4 base material.

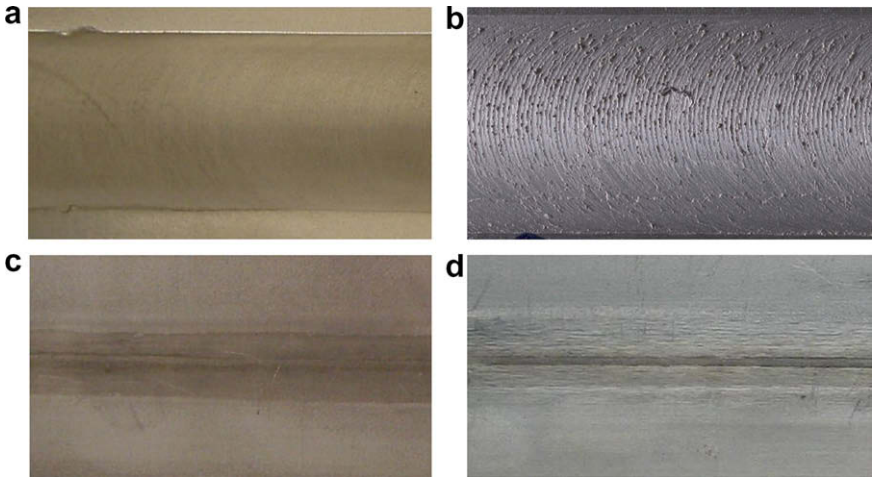

Fig. 3. Crown and route views of the welds HW (a and b) and CW (c and d).

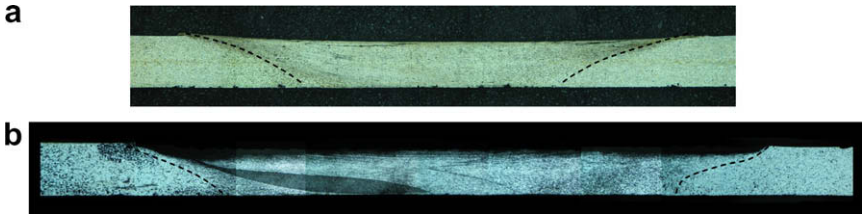

Fig. 4. Transverse cross-sections of the HW (a) and CW (b) welds.

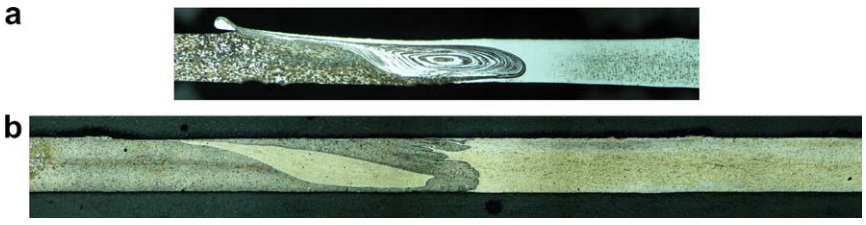

Fig. 5. Transverse cross-sections of dissimilar welds between alloys AA 5182-H111 (on the left) and AA 6016-T4 (on the right), welded with Tool 1 (a) and Tool 2 (b).

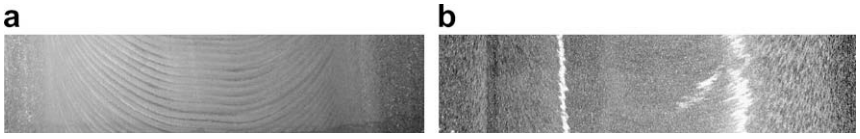

Fig. 6. Horizontal cross-sections of the welds CW (a) and HW (b).

welds, common features are more evident. In fact, a tongue of differently contrasted material, going upwards through the advancing side of the welds, is visible in both the similar and dissimilar welds. The chemical analysis of the CD welds enabled to conclude that this tongue results from the intense mixing of both base materials, which are severely plasticized around the pin during the welding process and dropped off, layer by layer, in the wake of the weld [64].

The similarities between the CW and CD welds suggest that the material flow mechanisms are analogous for both the similar and dissimilar welds, and so, the resulting macrostructures also have to be similar. In fact, since for the similar welds appropriate etching contrast results from differences in plastic deformation levels between the weld and the base material [65] or from different precipitation patterns [66], it is possible to assume that the dark tongue visible in the CW weld macrograph is a layer of highly plasticised material. In Fig. 6a is shown a horizontal cross-section of the CW weld in which arc shaped features, almost regularly spaced, which are characteristic of the periodic deposition of material at the trailing side of the FSW tool, can be seen. The spacing between the arcs corresponds to the tool advance per revolution as stated earlier by several authors [4,25,67–72].

For the welds produced with Tool 1, neither the onion ring structure is discernible in Fig. 4a, nor arc shape features are visible in the horizontal cross-section of the weld presented in Fig. 6b. Assuming that the flow of material is analogous during similar or dissimilar welding, an onion ring structure similar to that observable for the HD weld was expected. The low etching contrast

attained in the HW samples can be considered indicative of lower plastic deformation levels in the welds produced with Tool 1, relative to that produced with Tool 2, which is in agreement with the conclusions previously attained for the dissimilar welds [64]. Another remarking feature of the horizontal view of the HW in Fig. 6b is the presence, at the top surface of the weld, of traces of the zigzag oxide layer (bright lines). For the welds produced with Tool 2, which is provided with a scrolled shoulder that has a through thickness influence area and promotes intense plastic deformation at the top surface of the weld, the oxide arrays at the top of the weld are not visible in the horizontal cross-section of the weld (Fig. 6a). In fact, for the CW welds, a distinctly dark etched layer can be observed in this zone of the weld, in the transverse macrograph of Fig. 4b. This top layer of drastically plasticized material, similar to the dark tong material, can be wrongly confused with a strong thickness decrease in the under shoulder area of the CW welds.

Fig. 7a and b shows TEM bright field images from the middle of the nugget of the HW and CW welds, respectively. This images show that the mean grain size at the central part of the CW weld nugget (Fig. 7b) is much smaller than that of the HW weld nugget (Fig. 8b): the mean grain size of the recrystallised grains is 2 μm for the CW welds and 7 μm for the HW welds. Since recrystallised grain size depends on the amount of plastic deformation and heat input, being smaller for large amounts of deformation and small heat input, these results support the previous assumption of large plastic deformation levels and small heat input in the CW welds.

As for the base material, the TEM images of Fig. 7 show coarse precipitates randomly distributed inside the nugget grains of both welds. Comparing both figures it is evident that the quantity of the coarse particles is much higher in the CW welds than in the HW welds. From these results it is possible to presume that the temperature attained in the HW welds was sufficiently high to promote full solubilisation of the small cluster precipitates of the naturally

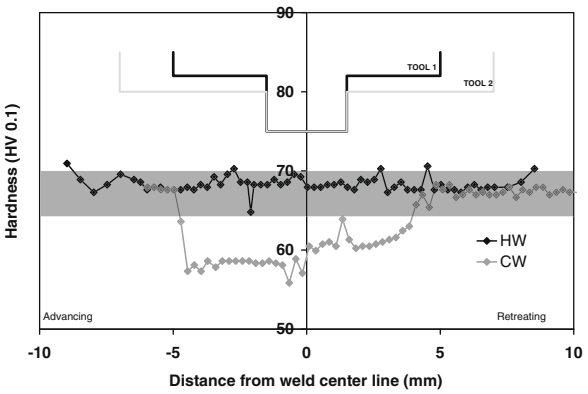

Fig. 8. Hardness profile across the HW and CW welds.

aged alloy. The post weld microstructure of the HW welds, which is very similar to that of the base material (Fig. 2), results from natural aging of a structure where the strengthening precipitates have been completely solubilised and is characterized by the presence of the randomly distributed coarse precipitates, probably not solubilised during the welding process due to the very rapid heating and cooling cycles. In the CW welds, assuming that the maximum temperature attained in the welding process is lower than that attained in the HW welds, it is possible that full solubilisation of strengthening precipitates was not possible. Small clusters solubilisation was accompanied by coarsening of larger precipitates, resulting in the overaged precipitate structure shown in Fig. 7b. This precipitation mechanism was proposed by some other authors to explain the softening in the HAZ of FS welds in other alloys of the 6XXX series [49,59,73]. The high density of coarse precipitates can be explained taking into account that the precipitation nucleation process in the stir zone is heterogeneous, with precipitates

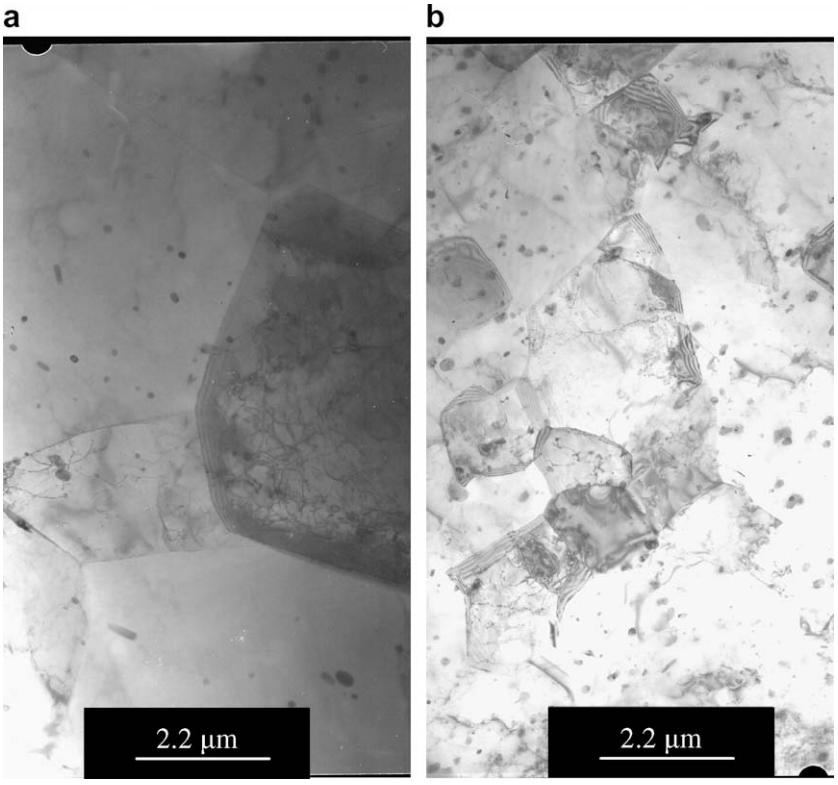

Fig. 7. TEM micrographs of the HW (a) and CW (b) weld nuggets.

nucleating randomly at dislocations and the extent of nucleation being strongly dependent on the dislocation density [54], which makes the highly plasticized CW material suitable for nucleation and coarsening of large precipitates. The grown of the coarse precipitates restrain further precipitation of small strengthening precipitates.

4.3. Mechanical testing

4.3.1. Hardness test results

The hardness profile evolution across the HW and CW welds is shown in Fig. 8. The horizontal gray bar represents the base material hardness that is scattered between 64 and 70 HV0.1. Sketches of the two welding tools were added in the figure in order to identify the under shoulder influence zone in each weld. The results plotted in the figure show very small differences in hardness between the HW weld and the base material and a strong decrease in hardness for the CW weld. The hardness decrease in the CW weld is clearly located under the toll shoulder area, between the advancing and retreating sides of the weld. The hardness values decrease abruptly, in the advancing side of the weld, and vary smoothly, from the weld centre line to the base material, in the retreating side of the weld.

Since the AA 6016-T4 alloy is a precipitation-hardenable alloy, it is well known that its mechanical properties are much more influenced by the volume fraction, size and distribution of strengthening precipitates than by the grain size in the stirred zone. So, according to the previous microstructural results, the hardening decrease in the CW weld is consistent with the coarse precipitates distribution depicted for this welds. The evenmatch hardening results between the HW welds and the base material is also consistent with the similarities in precipitate distribution that can be depicted by comparing Figs. 2 and 7a.

Sato et al. [2] joined the 6063-T4 aluminium alloy, by FSW, using different tool rotation speeds and a constant transverse speed. These authors found that the maximum temperature attained in the stir zone during the welding process, measured by using thermocouples, rose sharply with increasing rotation speed up to 2000 rpm. The grain size of the stir zone increased exponentially with increasing maximum temperature. These authors also found that the hardness values in the as-welded condition were distributed homogeneously in the weld and, contrarily to present results, they did not find significant differences in the hardness profiles registered for the welds produced with different tool rotation speeds. This suggests that the precipitation pattern that is responsible for the hardness decrease registered in present work for the CW, produced with low rotation speed, relative to the HW, produced with high rotation speed, is not only a consequence of the thermal cycle induced during the welding process, but was also influenced by the extreme plastic deformation levels induced by Tool 2, that conduct to a extremely refined grain structure (Fig. 7b). High density of coarse precipitates and grain boundaries are usually associated with the presence of precipitate free zones that adversely affect the mechanical and corrosion properties of the alloys.

In order to understand the unsymmetrical hardness distribution of the CW welds, a horizontal cross-section of a dissimilar CD weld, at 0.32 mm from the weld root, is shown in Fig. 9a.This cross-section includes the final hole left by the probe at the end of the weld. Different flow zones around the tool are identified in this horizontal section, namely, (1) is the advancing side material, (2) is a inner shear layer, surrounding the pin, that is constituted by the drastically plasticized material that originates the tongue visible in previous macrographs of the CW and CD welds, (3) is a layer of advancing side material, which is drawn from the advancing side of the weld, all around the tool, and is extruded against the inner shear layer at the back of the tool, and finally, (4) is the retreating side material that is drawn, from the front to the rear of the tool, almost parallel to the two inner flow layers. The different layers shown in this figure were subjected to different strain rates. Since the nucleation of coarse particles in the CW nugget was related to the dislocation density, it is reasonable to assume that there is a

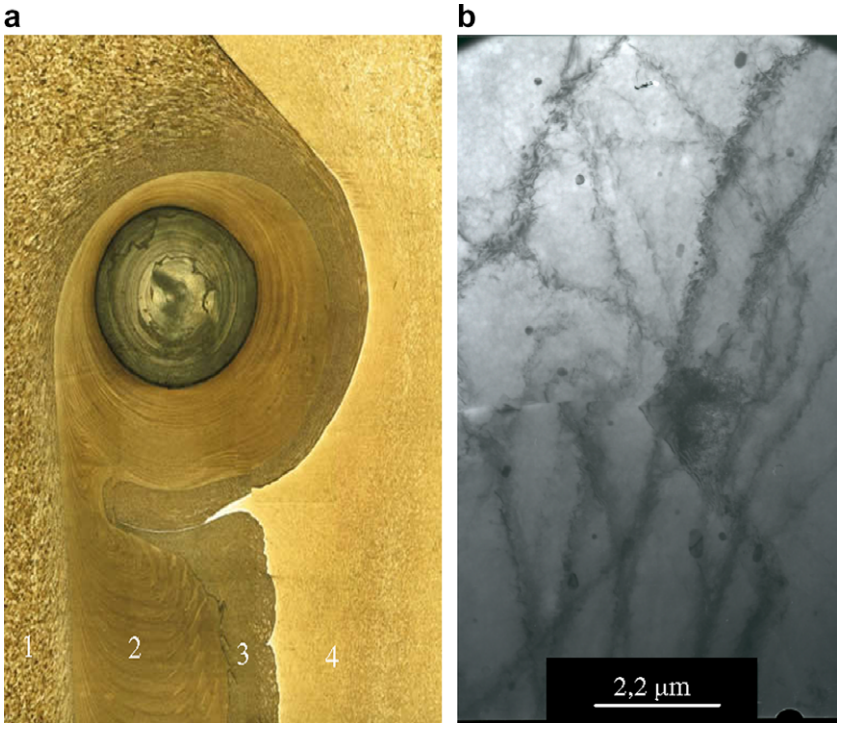

Fig. 9. Horizontal cross-section of a CD weld and TEM microstructure from (4) in image (a).

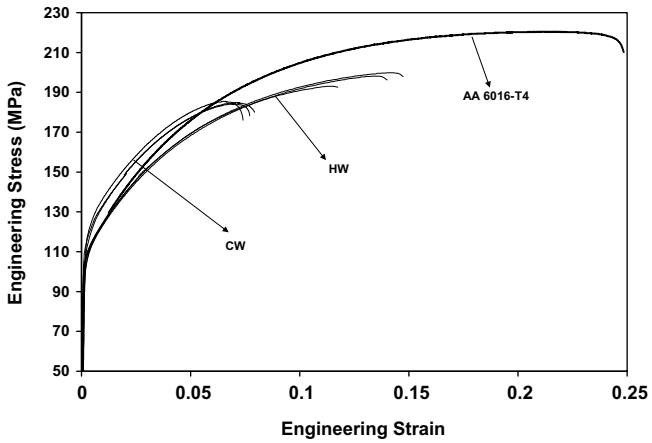

Fig. 10. Engineering stress/strain curves for the AA 6016-T4 base material and for HW and CW weld samples.

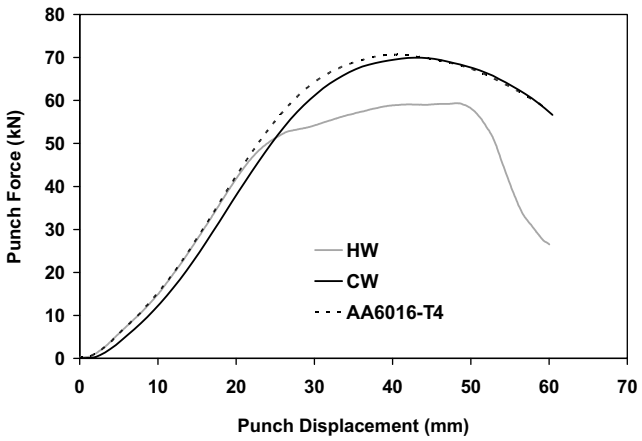

Fig. 12. Fig. 5 – Punch load–displacement curves.

gradient in plastic deformation from the inner shear layer to the outer retreating side material layer, which also leads to a gradient in coarse particle nucleation, and consequently, a gradient in hardness.

In Fig. 9b is shown a TEM bright field image sampling the microstructure at zone 4 in Fig. 9a. According to the hardness distribution in Fig. 8, this region of the weld, that is still located in the under shoulder area, has hardness values similar to that of the base material. The microstructure shown in the figure reveals a recovered grain structure with well defined dislocation walls and the same structure of randomly distributed coarse precipitates of the base material, which explains evenmatched hardness values. This non-recrystalized recovered microstructure is characteristic of the TMAZ of any FS weld and, despite not shown here, was observed in both the retreating and advancing sides of CW and HW welds.

4.3.2. Tensile test results

The stress–strain curves obtained in the tensile tests of base material (AA 6016-T4) and transverse weld samples (HW and CW) are plotted in Fig. 10. Since the deformation is highly heterogeneous in the transverse weld samples, the stress and strain values plotted in the graphs are engineering values calculated from the initial geometry of the samples. It is important to enhance the reproducibility of the weld tensile test results. The results reported in the graph show that despite the yield stress values are similar for both types of weld samples and for the base material, the global ductility of the weld samples is smaller than that of the base material.

The decrease in ductility of the CW weld samples relative to the base material is in accordance with previous results that reported severe hardness undermatch for these welds. For HW welds, the loss in ductility relative to the base material can be associated with the cross-section variation along the specimens gauge length due to the thickness reduction in the weld. In fact, despite it was registered a thickness undermatch of 0.1 mm in the HW welds, the engineering stresses and strains for the HW samples were plotted considering a constant cross-section, 1 mm thick, along the entire gauge length of the samples. From the results shown in Fig. 10, it is possible to conclude that the HW and CW welds have, respectively, 30% and 70% lower ductility than the base material.

4.3.3. Formability test results

Finally, the formability of the TWBs was assessed by deep-drawing axissymetric cups. The deep-drawing tests were performed using circular TWB specimens, with 200 mm diameter. The cylindrical cups obtained from the HW and CW blanks are shown in Fig. 11a and b, respectively. As it is shown in this figure, no rupture was observed in the welds for both types of TWBs, which confirms the good plastic deformation behaviour of either the evenmatched (HW) and undermatched (CW) welds. However, despite no rupture was registered, strong wrinkling occurred for the HW blanks.

In Fig. 12 are shown the punch force–displacement curves for the TWBs and an example of a punch force–displacement curve for a homogeneous base material blank. Analysing the graph it is possible to observe that, despite the undermatched mechanical properties registered for the CW welds, the punch force evolution for the CW blank is very similar to that of the base material. Concerning the evenmatched HW blanks, the punch force evolution is

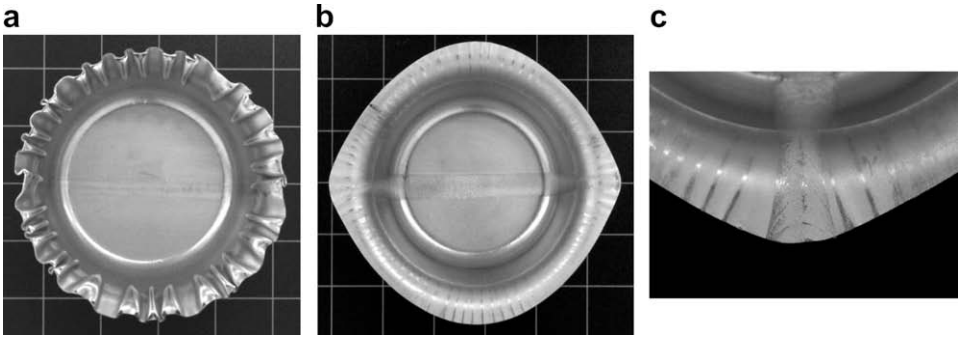

Fig. 11. Cylindrical cups obtained from HW (a) and CW (b and c) blanks.

very close to that of the base material, until around 20 mm punch displacement. After this, strong wrinkling started at the cup flanges, which was accompanied by a strong decrease in the punch force relative to the base material. The main cause for wrinkling is the deformation taking place in the zone between the die and the punch, where the workpiece is unsupported and tangential compressive stresses arise promoting buckling and folds. The absence of wrinkling in the case of the undermatched CW blanks, which were drawn under the same blank-holder force used for the HW blanks, can be explained by the plastic deformation of the softer weld material that avoids buckling. In fact, strong weld width variations along the cup walls can be observed in Fig. 11c where a magnification of the flange area in a CW cup is shown.

5. Conclusions

From the investigation done in the FS welds of very thin plates of the AA 6016-T4 aluminium alloy, it was concluded that the differences in tool geometry and welding parameters induced significant changes in the material flow path during welding as well as in the microstructure in the weld nugget.

The welds produced with the conical shoulder (HW) displayed a larger nugget grain size with few coarsened precipitates as opposed to the welds done with the scrolled shoulder (CW), which showed a smaller grain size containing many coarsened precipitates. These differences in microstructure conducted to a reduction in hardness around 15% in the CW welds contrarily to the HW welds where an evenmatch condition was reached.

A reduction in elongation of 30% and 70%, respectively, for the HW and CW welds was observed due to the microstructural alteration reported as well as to the thickness reduction registered in the HW welds. Despite the mechanical heterogeneity, the CW tailored blanks displayed good deep-drawing behaviour. Under the same deep-drawing conditions the evenmatched HW cups displayed strong wrinkling.

Acknowledgements

The authors are indebted to the Portuguese Foundation for the Science and Technology (FCT) and FEDER for the financial support through the POCI 2010 program and to Novelis Switzerland SA for supplying the aluminium sheets.

References

[2] Sato YS, Urata M, Kokawa H. Parameters controlling microstructure and hardness during friction-stir welding of precipitation-hardenable aluminum alloy 6063. Metall Mater Trans A 2002;33(3):625–35.
[3] Lim S, Kim S, Lee CG, Kim S-J. Tensile behavior of friction-stir-welded Al 6061-T651. Metall Mater Trans A 2004;35(9):2829–35.
[4] Yang B, Yan J, Sutton MA, Reynolds AP. Banded microstructure in AA2024-T351 and AA2524-T351 aluminum friction stir welds: Part I. Metallurgical studies. Mater Sci Eng A 2004;364(1–2):55–65.
[5] Peel MJ, Steuwer A, Withers PJ, Dickerson T, Shi Q, Shercliff H. Dissimilar friction stir welds in AA5083–AA6082. Part I: process parameter effects on thermal history and weld properties. Metall Mater Trans A 2006;37:2183–93.
[8] Dawes CJ, Thomas WM. Friction stir process welds aluminum alloys. Weld J 1996;75(3):41–5.
[9] Mishra RS, Ma ZY. Friction stir welding and processing. Mater Sci Eng R 2005;50(1–2):1–78.
[10] Feng AH, Ma ZY. Enhanced mechanical properties of Mg–Al–Zn cast alloy via friction stir processing. Scripta Mater 2007;56(5):397–400.
[11] Xie GM, Ma ZY, Geng L, Chen RS. Microstructural evolution and mechanical properties of friction stir welded Mg–Zn–Y–Zr alloy. Mater Sci Eng A 2007;471(1–2):63–8.
[12] Lee W-B, Jung S-B. The joint properties of copper by friction stir welding. Mater Lett 2004;58(6):1041–6.
[13] Sakthivel T, Mukhopadhyay J. Microstructure and mechanical properties of friction stir welded copper. J Mater Sci 2007;42(19):8126–9.
[14] Xie GM, Ma ZY, Geng L. Development of a fine-grained microstructure and the properties of a nugget zone in friction stir welded pure copper. Scripta Mater 2007;57(2):73–6.
[15] Fujii H, Cui L, Tsuji N, Maeda M, Nakata K, Nogi K. Friction stir welding of carbon steels. Mater Sci Eng A 2006;429(1–2):50–7.
[16] Hovanski Y, Santella ML, Grant GJ. Friction stir spot welding of hot-stamped boron steel. Scripta Mater 2007;57(9):873–6.
[17] Sato YS, Yamanoi H, Kokawa H, Furuhara T. Microstructural evolution of ultrahigh carbon steel during friction stir welding. Scripta Mater 2007;57(6):557–60.
[18] Ueji R, Fujii H, Cui L, Nishioka A, Kunishige K, Nogi K. Friction stir welding of ultrafine grained plain low-carbon steel formed by the martensite process. Mater Sci Eng A 2006;423(1–2):324–30.
[19] Lee W-B, Lee C-Y, Chang W-S, Yeon Y-M, Jung S-B. Microstructural investigation of friction stir welded pure titanium. Mater Lett 2005;59(26):3315–8.
[20] Reynolds AP, Hood E, Tang W. Texture in friction stir welds of Timetal 21S. Scripta Mater 2005;52(6):491–4.
[21] Feng AH, Ma ZY. Formation of Cu2FeAl7 phase in friction-stir-welded SiCp/Al–Cu–Mg composite. Scripta Mater 2007;57(12):1113–6.
[22] Storjohann D, Barabash OM, David SA, Sklad PS, Bloom EE, Babu SS. Fusion and friction stir welding of aluminum–metal–matrix composites. Metall Mater Trans A 2005;36(11):3237–47.
[23] Balasubramanian V. Relationship between base metal properties and friction stir welding process parameters. Mater Sci Eng A 2008;480(1–2):397–403.
[24] Fujii H, Cui L, Maeda M, Nogi K. Effect of tool shape on mechanical properties and microstructure of friction stir welded aluminum alloys. Mater Sci Eng A 2006;419(1–2):25–31.
[25] Krishnan KN. On the formation of onion rings in friction stir welds. Mater Sci Eng A 2002;327(2):246–51.
[26] Liu G, Murr LE, Niou CS, McClure JC, Vega FR. Microstructural aspects of the friction-stir welding of 6061-T6 aluminum. Scripta Mater 1997;37(3):355–61.
[27] Liu HJ, Fujii H, Maeda M, Nogi K. Tensile properties and fracture locations of friction-stir welded joints of 6061-T6 aluminum alloy. J Mater Sci Lett 2003;22(15):1061–3.
[28] Moreira PMGP, de Figueiredo MAV, de Castro PMST. Fatigue behaviour of FSW and MIG weldments for two aluminium alloys. Theor Appl Fract Mech 2007;48(2):169–77.
[29] Murr LE, Flores RD, Flores OV, McClure JC, Liu G, Brown D. Friction-stir welding: microstructural characterization. Mater Res Innov 1998;1(4):211–23.
[30] Murr LE, Liu G, McClure JC. A TEM study of precipitation and related microstructures in friction-stir-welded 6061 aluminium. J Mater Sci 1998;33(5):1243–51.
[31] Ren SR, Ma ZY, Chen LQ. Effect of welding parameters on tensile properties and fracture behavior of friction stir welded Al–Mg–Si alloy. Scripta Mater 2007;56(1):69–72.
[32] Lee W-B, Yeon Y-M, Jung S-B. The joint properties of dissimilar formed Al alloys by friction stir welding according to the fixed location of materials. Scripta Mater 2003;49(5):423–8.
[33] Li Y, Murr LE, McClure JC. Solid-state flow visualization in the friction-stir welding of 2024 Al to 6061 Al. Scripta Mater 1999;40(9):1041–6.
[34] Li Y, Murr LE, McClure JC. Flow visualization and residual microstructures associated with the friction-stir welding of 2024 aluminum to 6061 aluminum. Mater Sci Eng A 1999;271(1–2):213–23.
[35] Lim S, Kim S, Lee CG, Kim S-J. Tensile behavior of friction-stir-welded A356-T6/Al 6061-T651 bi-alloy plate. Metall Mater Trans A 2004;35(9):2837–43.
[36] Murr LE, Li Y, Flores RD, Trillo EA, McClure JC. Intercalation vortices and related microstructural features in the friction-stir welding of dissimilar metals. Mater Res Innov 1998;2(3):150–63.
[37] Prado RA, Murr LE, Soto KF, McClure JC. Self-optimization in tool wear for friction-stir welding of Al 6061 + 20% Al_2O_3 MMC. Mater Sci Eng A 2003;349(1–2):156–65.
[38] Shigematsu I, Kwon YJ, Suzuki K, Imai T, Saito N. Joining of 5083 and 6061 aluminum alloys by friction stir welding. J Mater Sci Lett 2003;22(5):353–6.
[39] Somasekharan AC, Murr LE. Microstructures in friction-stir welded dissimilar magnesium alloys and magnesium alloys to 6061-T6 aluminum alloy. Mater Charact 2004;52(1):49–64.
[40] Somasekharan AC, Murr LE. Characterization of complex, solid-state flow and mixing in the friction-stir welding (FSW) of aluminum alloy 6061-T6 to magnesium alloy AZ91D using color metallography. J Mater Sci 2006;41(16):5365–70.
[41] Buffa G, Donati L, Fratini L, Tomesani L. Solid state bonding in extrusion and FSW: process mechanics and analogies. J Mater Process Tech 2006;177(1–3):344–7.
[42] Minton T, Mynors DJ. Utilisation of engineering workshop equipment for friction stir welding. J Mater Process Tech 2006;177(1–3):336–9.
[43] Peel MJ, Steuwer A, Withers PJ. Dissimilar friction stir welds in AA5083–AA6082. Part II: process parameter effects on microstructure. Metall Mater Trans A 2006;37(7):2195–206.
[44] Scialpi A, De Filippis LAC, Cavaliere P. Influence of shoulder geometry on microstructure and mechanical properties of friction stir welded 6082 aluminium alloy. Mater Design 2007;28(4):1124–9.
[45] Scialpi A, De Giorgi M, De Filippis LAC, Nobile R, Panella FW. Mechanical analysis of ultra-thin friction stir welding joined sheets with dissimilar and similar materials. Mater Design 2008;29(5):928–36.
[46] Steuwer A, Peel MJ, Withers PJ. Dissimilar friction stir welds in AA5083–AA6082: the effect of process parameters on residual stress. Mater Sci Eng A 2006;441(1–2):187–96.
[47] Thomas WM, Nicholas ED. Friction stir welding for the transportation industries. Mater Design 1997;18(4–6):269–73.

[48] Muthukumaran S, Mukherjee SK. Two modes of metal flow phenomenon in friction stir welding process. Sci Technol Weld Joi 2006;11(3):337–40.
[49] Sato YS, Kokawa H, Enomoto M, Jogan S. Microstructural evolution of 6063 aluminum during friction-stir welding. Metall Mater Trans A 1999;30(9): 2429–37.
[50] Sato YS, Kokawa H, Ikeda K, Enomoto M, Hashimoto T, Jogan S. Microtexture in the friction-stir weld of an aluminum alloy. Metall Mater Trans A 2001;32(4):941–8.
[51] Sinha P, Muthukumaran S, Mukherjee SK. Analysis of first mode of metal transfer in friction stir welded plates by image processing technique. J Mater Process Tech 2008;197(1–3):17–21.
[52] Cabibbo M, McQueen HJ, Evangelista E, Spigarelli S, Di Paola M, Falchero A. Microstructure and mechanical property studies of AA6056 friction stir welded plate. Mater Sci Eng A 2007;460–461:86–94.
[53] Cabibbo M, Meccia E, Evangelista E. TEM analysis of a friction stir-welded butt joint of Al–Si–Mg alloys. Mater Chem Phys 2003;81(2–3):289–92.
[54] Olea CAW, Roldo L, dos Santos JF, Strohaecker TR. A sub-structural analysis of friction stir welded joints in an AA6056 Al-alloy in T4 and T6 temper conditions. Mater Sci Eng A 2007;454–455:52–62.
[55] Miles MP, Nelson TW, Decker BJ. Formability and strength of friction-stir-welded aluminum sheets. Metall Mater Trans A 2004;35(11):3461–8.
[56] Miles MP, Nelson TW, Melton DW. Formability of friction-stir-welded dissimilar-aluminum-alloy sheets. Metall Mater Trans A 2005;36(12):3335–42.
[57] Lee WB, Yeon YM, Jung SB. Evaluation of the microstructure and mechanical properties of friction stir welded 6005 aluminum alloy. Mater Sci Technol 2003;19(11):1513–8.
[58] Simar A, Bréchet Y, de Meester B, Denquin A, Pardoen T. Microstructure, local and global mechanical properties of friction stir welds in aluminium alloy 6005A-T6. Mater Sci Eng A 2008;486(1–2):85–95.
[59] Heinz B, Skrotzki B. Characterization of a friction-stir-welded aluminum alloy 6013. Metall Mater Trans B 2002;33(3):489–98.
[60] Giera A, Merklein M, Geiger M. Statistical investigations on friction stir welded aluminum tailored blanks for a robust process window advanced. Mater Res 2005;6–8:599–606.
[61] Rodrigues DM, Chaparro BM, Leitão C, Baptista AJ, Loureiro A, Vilaça P. Formability of steel and aluminium tailor welded blanks. Welding in the World 2007;51:667–76 [special issue].
[62] Leal RM, Chaparro BM, Antunes JM, Vilaça P, Rodrigues DM, Loureiro A. Mechanical behaviour of FSW aluminium tailored blanks. Mater Sci Forum 2008;587–588:961–5.
[63] Murayama M, Hono K. Pre-precipitate clusters and precipitation processes in Al–Mg–Si alloys. Acta Mater 1999;47(5):1537–48.
[64] Leal RM, Leitão C, Loureiro A, Rodrigues DM, Vilaça P. Material flow in heterogeneous friction stir welding of thin aluminium sheets: effect of shoulder geometry. Mater Sci Eng A 2008, in press. doi:10.1016/j.msea.2008.08.018.
[65] Okayasu M, Shin DH, Mizuno M. Effect of carbon content on etching response for identification of plastic deformation zones in carbon steels. Mater Sci Eng A 2008;474(1–2):140–7.
[66] Sutton MA, Yang B, Reynolds AP, Taylor R. Microstructural studies of friction stir welds in 2024-T3 aluminum. Mater Sci Eng A 2002;323(1–2):160–6.
[67] Chen ZW, Cui S. On the forming mechanism of banded structures in aluminium alloy friction stir welds. Scripta Mater 2008;58(5):417–20.
[68] Chen ZW, Pasang T, Qi Y. Shear flow and formation of Nugget zone during friction stir welding of aluminium alloy 5083-O. Mater Sci Eng A 2008;474(1–2):312–6.
[69] Kumar K, Kailas SV. The role of friction stir welding tool on material flow and weld formation. Mater Sci Eng A 2008;485(1–2):367–74.
[70] Reynolds AP. Flow visualization and simulation in FSW. Scripta Mater 2008;58(5):338–42.
[71] Schneider JA, Nunes Jr AC. Characterization of plastic flow and resulting microtextures in a friction stir weld. Metall Mater Trans B 2004;35: 777–83.
[72] Xu S, Deng X. A study of texture patterns in friction stir welds. Acta Mater 2008;56(6):1326–41.
[73] Sato YS, Kokawa H, Enomoto M, Jogan S, Hashimoto T. Precipitation sequence in friction stir weld of 6063 aluminum during aging. Metall Mater Trans A 1999;30(12):3125–30.